Chemotactic Separation of Enzymes

Krishna Kanti Dey,[†] Sambeeta Das,[†,§] Matthew F. Poyton,[†,§] Samudra Sengupta,[†] Peter J. Butler,[‡] Paul S. Cremer,[*,†] and Ayusman Sen[*,†]

[†]Department of Chemistry, [‡]Department of Biomedical Engineering, The Pennsylvania State University, University Park, Pennsylvania 16802, United States. [§]S.D. and M.F.P. contributed equally.

ABSTRACT We demonstrate a procedure for the separation of enzymes based on their chemotactic response toward an imposed substrate concentration gradient. The separation is observed within a two-inlet, five-outlet microfluidic network, designed to allow mixtures of active (ones that catalyze substrate turnover) and inactive (ones that do not catalyze substrate turnover) enzymes, labeled with different fluorophores, to flow through one of the inlets. Substrate solution prepared in phosphate buffer was introduced through the other inlet of the device at the same flow rate. The steady-state concentration profiles of the enzymes were obtained at specific positions within the outlets of the microchannel using fluorescence microscopy. In the presence of a substrate concentration gradient, active enzyme molecules migrated preferentially toward the substrate channel. The excess migration of the active enzyme molecules was quantified in terms of an enrichment coefficient. Experiments were carried out with different pairs of enzymes. Coupling the physics of laminar flow of liquid and molecular diffusion, multiphysics simulations were carried out to estimate the extent of the chemotactic separation. Our results show that, with appropriate microfluidic arrangement, molecular chemotaxis leads to spontaneous separation of active enzyme molecules from their inactive counterparts of similar charge and size.

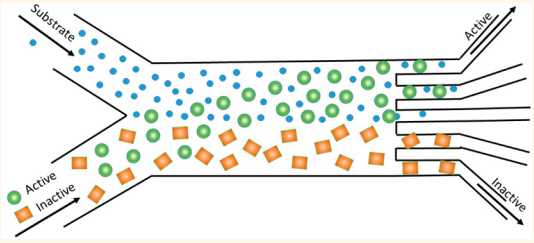

KEYWORDS: chemotaxis · nanomotor · catalysis · microfluidics · separation · enzyme

In vitro separation and isolation of active biomolecules plays a critical role in biological and biotechnological analyses associated with pathogen detection,[1] cancer cell identification,[2] mRNA isolation,[3] and tissue engineering,[4] among others. Recent advances in device miniaturization have led to the development of integrated lab-on-a-chip devices, offering a variety of simple and efficient separation techniques, dealing mostly with micron-scale particles.[5,6] Microfluidics has served as a prominent platform for the development of small, inexpensive and efficient diagnostic devices owing to their reduced reagent consumption rate and short sampling-to-result time.[7,8] Techniques for particle separation in microfluidic systems based on gravitational,[9] magnetic,[10] acoustic,[11] and electrokinetic forces[12] have been demonstrated. Although these protocols often lead to high throughput separation of micron scale particles, their use in biomolecular separations can damage the molecules due to stresses arising from external field-driven sieving and tweezing.[13] Moreover, conventional sorting chips usually involve polymeric gels within the outlets as sieving matrices,[14,15] which pose difficulties in multistep analysis in molecular separations.[16] Current label-free separation techniques, which rely on the differences in physical properties of particles such as shape,[17] density,[18] adhesion,[19] dielectric constant,[20,21] or diffusion[22] do not give efficient separation if these differences between the biomolecules in a complex mixture are not high.[19] The challenge therefore remains in harvesting specific biomolecules with very similar physical properties from a complex mixture, and in quantities that are sufficient for downstream sensing and detection.

Herein, we demonstrate the spontaneous separation of active from inactive enzymes, even with similar physical characteristics, *based solely on their catalytic activity*. Micro- and nanoscale catalytic motors have recently been the subject of intensive investigations because of their ability to negotiate complex environments.[23−26] These self-driven motors display collective directional migration toward targets under appropriate conditions,[27,28] suggesting interesting applications in fields ranging from fluidics[29] to surgery.[30] It has been demonstrated that like other catalytic motors, enzymes are also able to power their own motion by turnover of their respective substrates present in the ambient fluid.[31−33] This is manifested in

* Address correspondence to asen@psu.edu, psc11@psu.edu.

Received for review August 7, 2014 and accepted September 22, 2014.

Published online September 22, 2014
10.1021/nn504418u

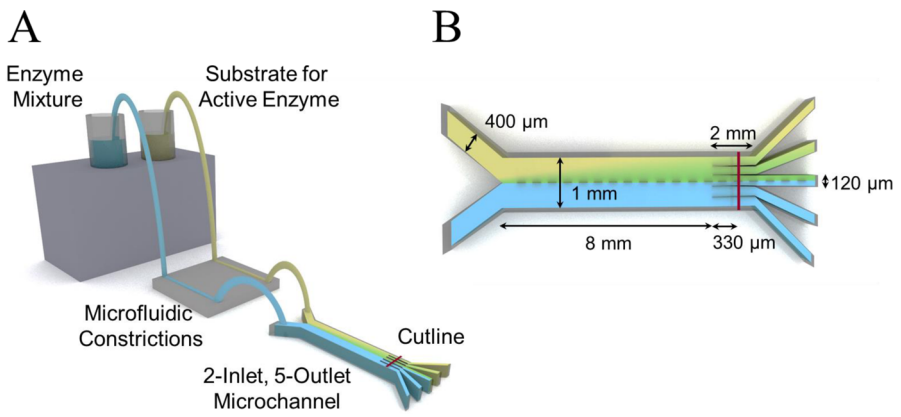

Figure 1. (A) Schematic of the experimental setup used to observe chemotactic separation of enzymes. (B) Dimensions of various sections of the microfluidic separator.

the form of substrate dependent enhancement in diffusivity. The precise mechanism for the turnover-induced enhanced diffusivity remains to be established. However, a number of mechanistic possibilities have been suggested. It has been proposed that enzymes can propel themselves in solution during substrate turnover by going through a sequence of nonreciprocal conformational changes during the substrate binding and product release steps.[34−36] Alternatively, Kapral has suggested that molecules can propel themselves through the generation of products that can interact with the enzymes *via* Lennard−Jones interaction potentials.[37] Spatially asymmetric catalysis can lead to inhomogeneous distribution of products. This nonhomogeneous product distribution creates a concentration gradient that can yield propulsion, depending on features of the products and the solvent. Finally, heat generation through reaction exothermicity can also lead to enhanced diffusion. However, in several instances the bulk rise in solution temperature due to enzymatic catalysis has been estimated and found to be in the micro-Kelvin range; too small to account for the observed enhanced diffusion.[38,39] Nevertheless, a local instantaneous reaction-induced rise in temperature cannot be ruled out at this point.

In the presence of a gradient in substrate concentration, the enzyme molecules migrate toward higher substrate concentration regions, a form of molecular chemotaxis.[38] We hypothesize that the chemotactic behavior of the enzyme molecules arises from the enhanced diffusion mechanism. The substrate concentration changes continuously as the enzyme diffuses along the gradient. Thus, at every point in space, the diffusivity increases on moving up the gradient and decreases on moving down the gradient. A higher diffusion coefficient leads to a greater spreading of the enzyme molecules on the side of the higher substrate concentration. Thus, the "center of gravity" of the enzyme ensemble moves toward higher substrate concentration. As with any nonequilibrium system, a continuous energy input is required for the directional movement, in this case to maintain the substrate gradient. The proposed mechanism is stochastic in nature and is different from biological chemotaxis, which requires temporal memory of the concentration gradient.

The *chemotactic* migration of enzymes toward areas of higher substrate concentration was utilized to separate enzymes from one another in a microfluidic device. The separation was monitored on-chip with a fluorescence microscope and the separated enzymes were collected through different outlets continuously during the process. Figure 1 shows a schematic diagram of the two-inlet, five outlet microfluidic setup used in experiments. Using the microfluidic separator, we were able to separate molecules of catalase from urease, urease from β-galactosidase, and active catalase from its inactive form. The separation efficiency of the device agrees well with finite element simulations of convective diffusion developed using COMSOL Multiphysics software. The proposed separation strategy does not depend on the size or charge of the molecules, and can be carried out under near ambient conditions needed for enzyme activity. Separation based on molecular chemotaxis through substrate turnover should allow enhanced sensitivity for point-of-need assays due to minimum influence of contaminants.

RESULTS AND DISCUSSION

Proof of Concept Studies. We used mixtures of catalase and urease, urease and β-galactosidase, and active and inactive catalase to demonstrate the separation of active biomolecules in the presence of their specific substrates. Each of these pairs of enzymes was carefully chosen to determine the relative merit of chemotactic sorting. It should be noted that the current method can be employed for any combinations of enzymes or other active molecules exhibiting high catalytic activity. For proof of concept studies, the above combinations were selected because of the high substrate turnover rates for catalase ($k_{cat} = 2.12 \times 10^5$ s^{-1})[40] and urease

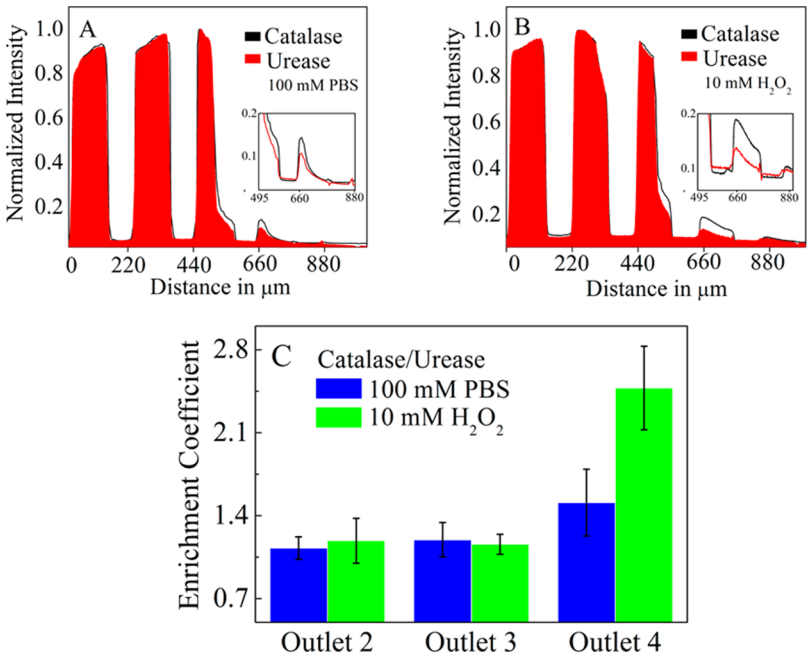

Figure 2. Separation of catalase from urease. Normalized fluorescence intensity profiles of the enzymes in the presence of (A) phosphate buffer and (B) imposed H_2O_2 concentration gradient. The profiles were recorded within the outlets along a cutline, at a distance of approximately 330 μm away from the split. The images in the insets show the magnified view of the fluorescence profiles near the third and fourth outlets of the device. (C) Measured enrichment coefficients of catalase and urease within different outlets of the device. The mean and standard deviations are calculated for three sets of independent observations, each carried out with a newly fabricated device.

($k_{cat} = 2.34 \times 10^4\ s^{-1}$).[41] For separation of catalase from urease, a 1:1 mixture of catalase and urease (each 200 nM) was allowed to flow through one of the inlets of a bovine serum albumin (BSA)-treated microchannel at 15 μL/h and a flow of phosphate buffer through the other at the same rate. After the flow had stabilized, the flow profiles of liquids near the inlet and outlets of the microchannel device were checked for uniformity. Typical flow profiles obtained at the inlets and near the outlet splits, for the two tagged enzymes are shown in Figure S1 of Supporting Information (SI). The fluorescence intensity profiles of the labeled enzymes were recorded within the outlets along a *cutline*, drawn across the outlets 330 μm down from the splits (Figure 1). Next, the flow of phosphate buffer was withdrawn from the channel and buffered solution with 10 mM H_2O_2 (substrate for catalase) was introduced at the same inlet, keeping the flow rate unaltered. After the flow had stabilized, the fluorescence intensity profiles of the enzymes were recorded along the same cutline. The measured intensity profiles were corrected for vignetting using nonlinear curve fits, adjusted for baselines and normalized before they were compared. In order to quantify the excess migration of catalase in the presence of H_2O_2, we follow the conventional definition of *enrichment coefficient*, the normalized concentration ratio of active to inactive molecules in a particular outlet channel divided by the same ratio at the inlet (= 1 in our setup).[42] For each enzyme, its concentration at the outlet is proportional to the geometrical area under its fluorescence intensity profile (as shown in Figure S2 in SI). We therefore calculated the fluorescence intensity profiles for each enzymes (after normalizing for differences in fluorophore intensities) within different outlets of the microchannel.

Figure 2(A–C) shows normalized intensity profiles for catalase and urease, measured along the specified cutline, in the presence of a flow of pure buffer and one with 10 mM H_2O_2, respectively. The magnified view of the intensity profiles measured from the middle of the third outlet to the end of the fourth (where the substrate concentration gradient is expected to be the maximum), are shown in the insets. In the absence of H_2O_2, the area under the intensity profile of catalase was found to be slightly more than that of urease toward the substrate side, starting from the middle of the third outlet and becoming the maximum within the fourth. This difference in migration can be attributed to the normal size-dependent Brownian diffusion of the molecules ($D_{catalase} = 6.01 \times 10^{-11}\ m^2/s$, $D_{urease} = 3.18 \times 10^{-11}\ m^2/s$).[38] However, in the presence of a substrate concentration gradient, the intensity corresponding to catalase becomes significantly higher than that of urease. The increase in measured enrichment coefficients in absence and presence of H_2O_2 is shown in Figure 2(C).

Unlike catalase and urease which are somewhat different in size, we next selected a mixture of two enzymes with similar Stokes radii, urease and

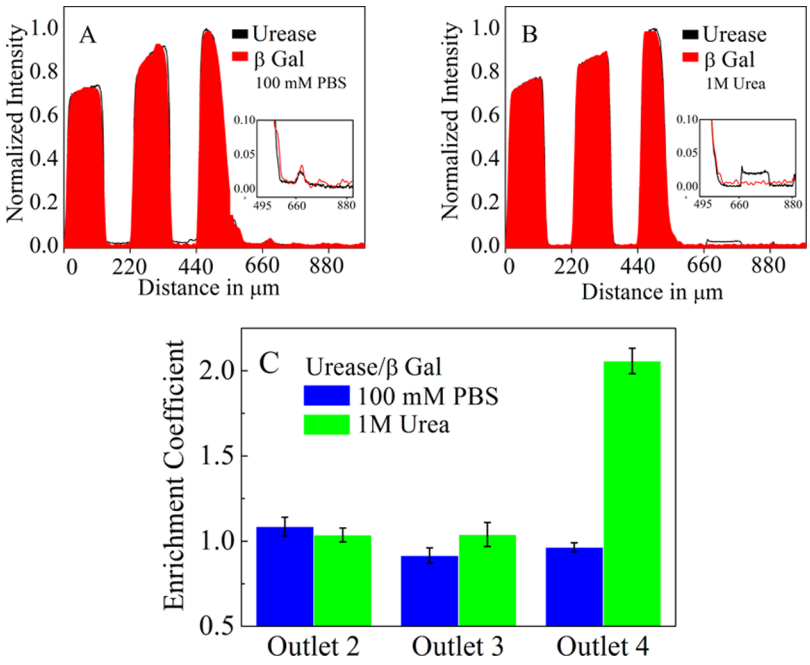

Figure 3. Separation of urease from β-galactosidase. Normalized fluorescence intensity profiles of the enzymes in the presence of (A) phosphate buffer, (B) imposed urea concentration gradient. The profiles were recorded within the outlets along a cutline, at a distance of approximately 330 μm away from the split. The images in the insets show the magnified view of the fluorescence profiles near the third and fourth outlets of the device. (C) Measured enrichment coefficients of urease and β-galactosidase within different outlets of the device. The mean and standard deviations are calculated for three sets of independent observations, each carried out with a newly fabricated device.

β-galactosidase (R_{urease} = 7 nm[31] and $R_{\beta\text{-galactosidase}}$ = 6.9 nm[43]) and demonstrated spontaneous separation of urease in the presence of a steady concentration gradient of urea. After preparing 200 nM protein solutions and washing the microchannels thoroughly with BSA and phosphate buffer as before, the separation experiments were performed with a liquid flow rate of ~15 μL/h at the inlets. The fluorescence intensity profiles of the enzymes were recorded within the outlets, in the presence and absence of a flow of substrate, which in this case was a buffered solution of 1 M urea. Figure 3(A–C) show normalized fluorescence intensity profiles of urease and β-galactosidase in absence/presence of a urea gradient, and the measured enrichment coefficients calculated for different outlets of the microfluidic device. The magnified views of the separation profiles are shown in the insets of Figure 3(A,B).

In the absence of urea, both urease and β-galactosidase moved almost identically, the latter migrating a little faster possibly because of its marginally higher Brownian diffusivity. In the presence of substrate, however, the population of urease increased in the direction toward the substrate side, following the enhanced diffusion of the molecules in the presence of a urea concentration gradient. Figure 3(C) shows the relative increase in urease population within different outlet channels of the device, in the presence and absence of urea. The observations clearly establish that by the appropriate choice of substrate, specific enzyme molecules can be chemotactically separated out from a complex mixture, without influencing any of their physical or chemical characteristics.

Sensitivity of Chemotactic Separation. Extending the idea of working with molecules of same Stokes radii, we finally probed the sensitivity of the technique in separating out active molecules from their inactive forms, both having the same size and isoelectric point. As discussed earlier, one of the major challenges facing current molecular separation techniques is dealing with proteins with nearly identical physical properties. To demonstrate the unique advantage of chemotactic separation over others, we chose a mixture of active and inactive catalase molecules and demonstrated their separation in the presence of an imposed H_2O_2 gradient. For this study, molecules of catalase were labeled separately with AF 647 and AF 488 dyes. Enzymes labeled with AF 488 were then inhibited using 0.5 M NaCN solution prepared in deionized water, the details of which are given in the SI. Solutions of active and inactive catalase were prepared in phosphate buffer keeping their individual concentrations fixed at 200 nM. Newly fabricated microchannels were treated with BSA and washed with flows of phosphate buffer prior to the measurements. The liquid flow rate was maintained at ~15 μL/h as before to ensure smooth laminar flow inside the main channel. Following the experimental protocol described previously, the intensity profiles of the enzymes, both in presence and absence of the substrate (solution of 10 mM H_2O_2)

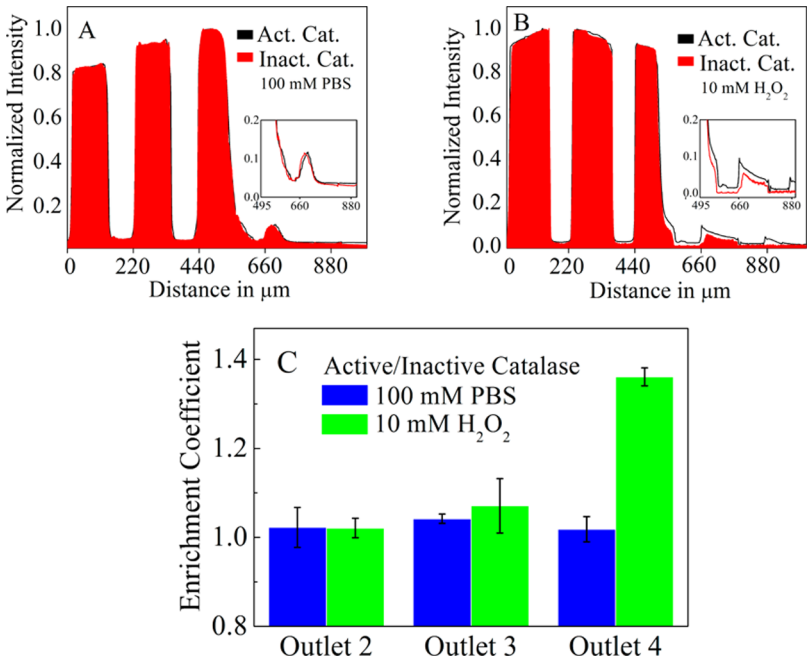

Figure 4. Separation of active and inactive catalase. Normalized fluorescence intensity profiles of the enzymes in the presence of (A) phosphate buffer, (B) imposed H_2O_2 concentration gradient. The profiles were recorded within the outlets along a cutline, at a distance of approximately 330 μm away from the split. The images in the insets show the magnified view of the fluorescence profiles near the third and fourth outlets of the device. (C) Relative enrichment coefficients of the molecules measured within different outlets of the device. The mean and standard deviations are calculated for three sets of independent observations, each carried out with a newly fabricated device.

were recorded within the outlets along the cutline. Figure 4(A,B) shows the normalized fluorescence intensity profiles of the enzymes, both in the presence and absence of 10 mM H_2O_2. Figure 4(C) shows the measured enrichment coefficients, for different outlets of the device averaged over three sets of independent measurements. As shown, there is a significant increase in the population of active catalase within the substrate outlets. As expected, the enrichment is observed to be mostly within the region between third and the fourth outlets, where the established substrate concentration gradient is the highest. Clearly, the chemotactic separation technique is sensitive enough to sort out molecules possessing identical physical properties, which cannot otherwise be accomplished using currently known separation techniques.

Multiphysics Simulations. In order to understand the observed chemotactic separation of enzymes, we propose a simple model describing diffusive and convective transport of enzymes in imposed substrate concentration gradients. The observed enrichment of molecules within the microfluidic channels was simulated in COMSOL multiphysics (v. 4.3), coupling the physics of diffusion of molecular species and principles of laminar flow. The simulation geometry followed the microchannel network used in experiments. The computations were performed in shallow channel approximation, where the simulation contour was assigned a depth of 50 μm, equal to the depth of the microchannels used in experiments. After deciding the domain, one of the inlets of the main channel was assigned a substrate flow rate of 15 μL/h, the same flow rate used in experiments. A solution containing a mixture of enzymes was then considered to flow through the other inlet of the microchannel at the same rate. The concentration of each enzyme in the mixture was taken to be 200 nM. This was followed by setting the boundary conditions and initial parameters, the details of which are described in the SI. The diffusion coefficients of inactive enzymes (enzymes not interacting with substrates) were dictated by their hydrodynamic radii and solution viscosity, and were considered constant in the simulation. The diffusion coefficients of active enzymes were, however, expressed as functions of local substrate concentrations, the functional forms of which were taken from previously reported results[38] and used in simulations as input parameters (for details, see SI). After calibrating the simulation mesh for fluid dynamics modeling, the steady-state concentration profiles of the enzymes were measured within the outlets, at a position 330 μm away from the split, along a cutline, drawn across the outlets. Simulations were done for different pairs of enzymes, in the presence and absence of corresponding substrates. Control experiments were simulated by assuming flow of phosphate buffer through the substrate inlet at the rate of ~15 μL/h, and assuming constant diffusivities of the molecules dictated by their hydrodynamic radii. Figure 5 summarizes

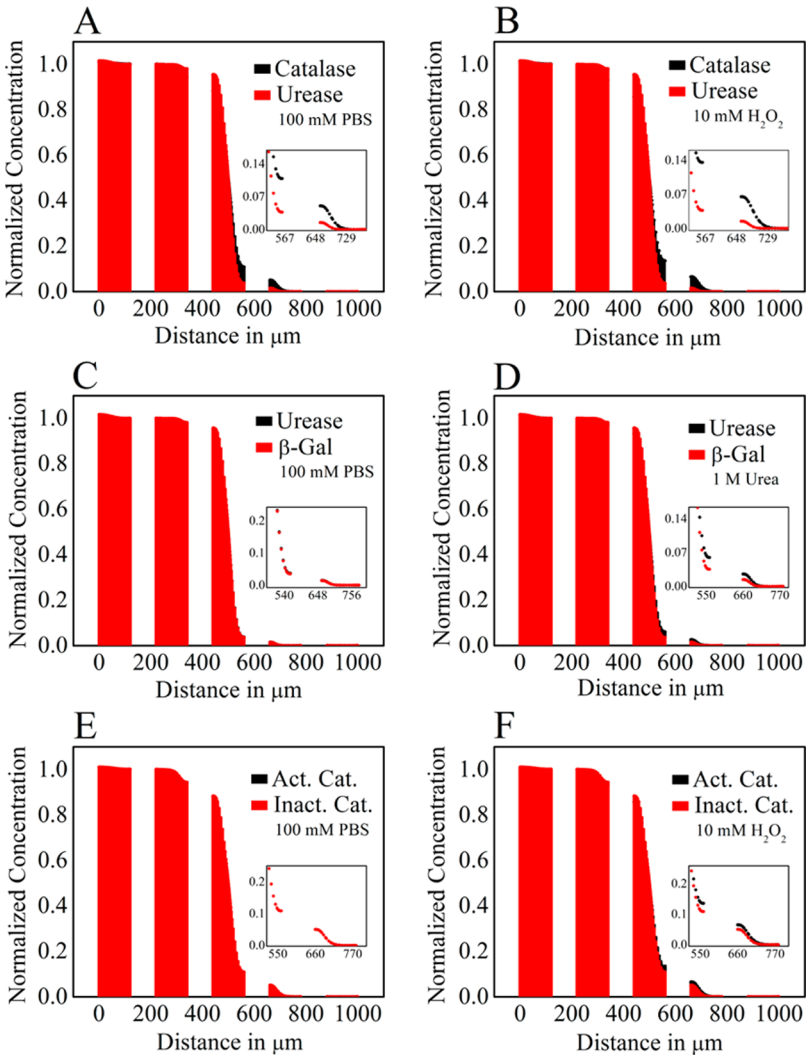

Figure 5. Simulated separation of enzymes in the presence of substrates. Normalized concentration profiles of catalase and urease in the presence of (A) phosphate buffer, (B) imposed H_2O_2 concentration gradient; urease and β-galactosidase in the presence of (C) phosphate buffer, (D) imposed urea concentration gradient; active and inactive catalase in the presence of (E) phosphate buffer, (F) imposed H_2O_2 concentration gradient. The images in the insets show the magnified view of the fluorescence profiles near the third and fourth outlets of the device. The concentration profiles are estimated within the outlets, along a cutline 330 μm away from the outlet splits.

the simulation results obtained for different pairs of enzymes under different experimental conditions.

For a mixture of catalase and urease, the simulation results show enrichment in catalase population within the outlets, in the presence of the substrate H_2O_2. The simulated enrichment coefficients for catalase within the third and fourth outlets of the microfluidic device are 1.00 and 6.41 in the presence of 10 mM H_2O_2 (compared to 1.01 and 4.04 in phosphate buffer) (see SI for details). Interestingly, the values indicate that the enrichment coefficient for catalase/urease system within the fourth outlet increases to 4 even in the absence of the substrate for catalase, indicating that the molecules can be separated solely based on size. However, addition of the substrate for catalase increases this enrichment coefficient by 58% to 6.41, demonstrating the utility of enhanced separation by molecular chemotaxis. The corresponding experimentally measured values of enrichment coefficients for catalase/urease systems are 1.16 $\pm$ 0.09 and 2.48 $\pm$ 0.35 in H_2O_2 (compared to 1.20 $\pm$ 0.14 and 1.51 $\pm$ 0.28 in buffer). Possible factors contributing to the difference in simulated and experimental values are errors involved in the nonlinear fitting of experimental data for substrate dependent diffusivities of the molecules, uncertainties in integrated areas under the fluorescence and concentration profiles, baseline corrections and related processing of measured signals and nonideal behavior of the PDMS microchannels under given experimental conditions. However, for the other pairs of enzymes, the estimated separation coefficients agree well with the experimentally observed values. For example, for urease and β-galactosidase the predicted enrichment coefficients within the third and fourth outlets are 1.00 and 2.04 in the presence of urea (compared to 1.00 and 0.97 in buffer). Experimental enrichment coefficients,

averaged over three independent sets of measurements were calculated to be 1.04 ± 0.04 and 2.06 ± 0.07 in the presence of urea, while those for the controls were 0.92 ± 0.04 and 0.96 ± 0.03, respectively. For active and inactive catalase, the estimated enrichment coefficients are 1.06 and 1.44 respectively compared to 1.00 and 1.00 in buffer. The experimental values matched well with the estimated ones—the measured values being 1.07 ± 0.06 and 1.36 ± 0.02 in the presence of 10 mM H_2O_2 (compared to 1.04 ± 0.01 and 1.02 ± 0.03 in buffer). Details of multiphysics simulations and estimated enrichment coefficients are provided in the SI.

Although the multiphysics simulations performed do not take into consideration factors such as backflow of fluids within the outlets and possible mixing near the splits, the results successfully predict the experimental observations and provide a basic model to understand chemotactic separation of enzymes in the presence of imposed substrate concentration gradients. Although a relatively simple microchannel setup was employed, more efficient separation will require a complex tree-like architecture (resulting in higher theoretical plates).[44] Increasing the concentrations of enzymes at the inlets would most likely result in higher number of molecules migrating within the substrate outlets, improving the efficiency of separation even further. With appropriate detection setups, the microchannel geometry may be modified further to sort out specific molecules at desired locations. The present two-inlet, five-outlet geometry however establishes the principle of chemotactic separation of molecules and demonstrates its applicability in sorting out molecules with identical physical properties. This cannot be achieved with current label-free detection and separation procedures and will provide avenues for efficient chemical and biochemical sorting of active molecules.

CONCLUSION

We have demonstrated a technique for the spontaneous sorting of enzymes that is based on substrate concentration-dependent diffusivity of active enzyme molecules and their chemotactic response toward imposed substrate gradients. Unlike other label-free techniques, chemotactic separation does not depend on physical properties, such as molecular size and surface charge. To validate our experimental observations, we estimated theoretical separation efficiencies for the given pairs of enzymes using multiphysics simulations in COMSOL. The simulated results matched well with the experimental results. In principle, the same technique can be used to separate out other active catalysts from their less active or inactive counterparts in the presence of their respective substrates and should, therefore, find wide applicability.

METHODS

Microchannel Architecture. The microfluidic channels were fabricated following standard soft lithography techniques,[45,46] the details of which are provided in the Supporting Information (SI). The main channel of the microfluidic chamber has a length of 8 mm, with a depth of 50 μm. Each of the inlets has a width of ~400 μm while the individual outlets were 120 μm wide. These dimensions ensured minimum interference of signals within adjacent outlets of the device. Before starting the experiments, a buffered solution of bovine serum albumin (BSA, 10 mg/mL) was allowed to flow through the device for about 20 min to minimize sticking of enzymes on the polydimethylsiloxane (PDMS) surface. This was followed by flows of 100 mM phosphate buffer from reservoirs held at approximately 10 cm above the microscope stage through both the inlets. With intermediate constrictions (consisting of parallel PDMS microchannels, each of width ~100 μm), the mixture of enzymes from a separate reservoir was then introduced through one of the inlets of the microchannel at a constant flow rate. The flow rate of liquid through the inlets and hence through the main channel can be controlled by changing the height of the liquid reservoirs. The concentrations of the two enzymes in the mixture were kept the same and they were labeled separately with different fluorescent dyes (for details, see SI). When there was no substrate, the flow of phosphate buffer through the other inlet was maintained at a rate equal to that of the enzyme solution. The flow profile was allowed to stabilize and fluorescence profiles of the enzymes were recorded along a *cutline*, drawn across the outlets 330 μm down from the split (Figure 1). The cutline was selected at a position sufficiently away from the split in order to minimize perturbation in fluorescence near the junction of the outlets. For chemotactic separation of enzymes, the phosphate buffer was replaced by a buffered solution of the substrate (corresponding to the active enzyme to be separated) flowing through the same inlet at the same rate. In the given microchannel architecture (Figure 1), the interface between the two flows runs through the middle of the third outlet of the device. Hence, the substrate gradient is expected to be maximum between the third and fourth outlets. In the presence of a substrate flow, the intensity profiles were again recorded along the same cutline within the outlets and compared.

Fluorescence Measurements. The fluorescence signal from the tagged enzymes was monitored and recorded using highly sensitive fluorescence imaging. The optical setup involved a Nikon Eclipse Ti inverted microscope with a 100 W halogen lamp. Excitation light was passed through the appropriate filter cube (Nikon), depending on the excitation/emission wavelengths of the tagged fluorophores, before it was focused onto the sample through 4x/10x objectives (Plan Apo 4×-0.20/Plan Apo 10×-0.45, Nikon). Fluorescence emission collected by the objective lens, was passed through interference filters, and detected by a sensitive iKon-M 934 CCD camera (Andor Technology) with a resolution of 1024 × 1024 pixels and maximum quantum efficiency of 95%.

Separation Experiments. For separation of catalase from urease, samples of bovine liver catalase (Sigma-Aldrich) and Jack bean urease (Sigma-Aldrich) were labeled with amine reactive fluorophores Alexa Fluor 647 (AF 647; ex/em: 650/668; Life Technologies Corporation) and Alexa Fluor 488 (AF 488; ex/em: 494/519; Life Technologies Corporation) dye, respectively. For separation of urease from β-galactosidase, samples of β-galactosidase (from *Escherichia coli*, Sigma-Aldrich) and Jack bean urease (Sigma-Aldrich) were labeled with AF 488 and AF 647, respectively. For separation of active catalase from its inactive counterpart, molecules of catalase were labeled separately with AF 647 and AF 488 dyes. Catalase molecules labeled

with AF 488 were then inhibited using 0.5 M NaCN solution prepared in deionized water. The details of protein labeling and inhibition are provided in the SI.

The fluorophores used in labeling are selected to ensure minimal overlap in their spectral profiles and hence possibility of any fluorescence resonance energy transfer (FRET) between the molecules. The concentrations of the labeled enzymes solutions were calculated using UV−vis measurements. A mixture of these enzymes was prepared in phosphate buffer, keeping their individual concentration fixed at 200 nM. Concentrations higher than 200 nM were often found to saturate the fluorescence detector while concentrations lower than 200 nM lowered the extent of chemotaxis. Further, separation of enzymes in the presence of their substrate concentration gradients is dependent on the duration of enzyme−substrate interaction. More enzyme molecules should be separated if they are allowed to spend more time between the inlets and the outlets of the microfluidic device. As such, the flow rate of the enzyme and substrate solutions through the microfluidic device should be slow enough to maximize the enzymes' ability to diffuse into the substrate channel. In view of this, prior to experimental measurements, we optimized the flow rate for 200 nM enzyme solutions based on Multiphysics simulations in COMSOL. Considering a mixture of active and inactive catalase, the excess migration of active catalase was estimated within the substrate outlets, in the presence of its substrate, 10 mM H_2O_2, for flow speeds ranging from 0.5 μm/s (~0.0375 μL/h) to 3000 μm/s (~225 μL/h). For very low liquid velocities (0.5 μm/s), the simulation showed no substrate concentration gradient along the interface of the flows (see Figure S6 in SI); the population of both active and inactive molecules was found to be the same within each of the outlets, resulting in no separation. The separation was significant above a flow speed of 20 μm/s and increased continuously with the increase in flow rate at the inlets (see Figure S7(C) in the SI). However, for flow rates higher than 200 μm/s (~15 μL/h), the concentration of enzymes crossing the substrate interface was found to be $<10^{-4}$ nM for both active and inactive catalase, making the detection of excess migration of the active molecules with respect to the inactive ones challenging. The details of the simulation results are provided in the SI. The detection of chemotactic separation is therefore very sensitive to the flow rate of liquids through the inlets. With more concentrated enzyme solutions, it may be possible to work with an extended range of flow rates, but as mentioned previously, higher concentrations of tagged enzymes saturated the fluorescence detector in the present experimental setup. On the basis of the simulation results, for 200 nM enzyme solutions, we decided to work with flow speeds close to 15 μL/h. However, obtaining slow flow rates exhibiting smooth laminar profiles in channels that have dimensions on the order of micrometers is challenging. While a syringe pump can pump fluid slowly (down to tens of microliters per hour) the observed flow was not smooth. As such, we used a gravity-driven flow by placing the enzyme and substrate reservoirs shown in Figure 1 at a higher height than the outlets of the microfluidic device. In order to further slow the flow rate, we placed a second microfluidic device with smaller channel dimensions (~100 μm) between the reservoirs and the separator to act as constrictions. This microfluidic cascade helped to attain smooth, gravity-driven laminar flow at the inlets at a rate of ~15 μL/h. This flow rate is orders of magnitude smaller than the flow rates typically used in microfluidic experiments.[6]

Conflict of Interest: The authors declare no competing financial interest.

Acknowledgment. We acknowledge the Research Computing and Cyber infra-structure unit of Information Technology Services at The Pennsylvania State University for providing advanced computing resources and services that have contributed to the research results reported in this paper (URL: http://rcc.its.psu.edu). Fabrication of microfluidic channels was carried out in the Nanofabrication Laboratory of Materials Research Institute, Penn State (under The National Nanotechnology Infrastructure Network (NNIN), supported by NSF). We thank Penn State MRSEC under NSF Grant DMR-0820404 for financial support. P.J.B. and P.S.C. also acknowledge financial support from NSF Grant CMMI 1334847. We thank Isamar Ortiz-Rivera for her help in designing the schematics. P.S.C. also thanks the Office of Naval Research (N00014-14-1-0792) for financial support.

Supporting Information Available: Fabrication of microfluidic channels, details of protein labeling with amine-reactive fluorophores, inhibition of active catalase, correlation between fluorescence and concentration of protein-dye conjugates, COMSOL multiphysics simulations on flow optimization and estimated separation, and data on substrate concentration dependent enzyme diffusivities. This material is available free of charge *via* the Internet at http://pubs.acs.org.

REFERENCES AND NOTES

1. Leonard, P.; Hearty, S.; Brennan, J.; Dunne, L.; Quinn, J.; Chakraborty, T.; O'Kennedy, R. Advances in Biosensors for Detection of Pathogens in Food and Water. *Enzym. Microb. Technol.* **2003**, *32*, 3–13.
2. Chen, J.; Li, J.; Sun, Y. Microfluidic Approaches for Cancer Cell Detection, Characterization, and Separation. *Lab Chip* **2012**, *12*, 1753–1767.
3. Reinholt, S. J.; Behrent, A.; Greene, C.; Kalfe, A.; Baeumner, A. J. Isolation and Amplification of mRNA within a Simple Microfluidic Lab on a Chip. *Anal. Chem.* **2014**, *86*, 849–856.
4. Nae, S.; Bordeianu, I.; Stăncioiu, A. T.; Antohi, N. Human Adipose-derived Stem Cells: Definition, Isolation, Tissue-Engineering Applications. *Rom. J. Morphol. Embryol.* **2013**, *54* (4), 919–924.
5. Lenshof, A.; Laurell, T. Continuous Separation of Cells and Particles in Microfluidic Systems. *Chem. Soc. Rev.* **2010**, *39*, 1203–1217.
6. Foudeh, A. M.; Didar, T. F.; Veresa, T.; Tabrizian, M. Microfluidic Designs and Techniques using Lab-on-a-Chip Devices for Pathogen Detection for Point-of-Care Diagnostics. *Lab Chip* **2012**, *12*, 3249–3266.
7. Li, Y.; Xu, F.; Liu, C.; Xu, Y.; Feng, X.; Liu, B. A Novel Microfluidic Mixer based on Dual-Hydrodynamic Focusing for Interrogating the Kinetics of DNA−Protein Interaction. *Analyst* **2013**, *138*, 4475–4482.
8. Atalay, Y. T.; Witters, D.; Vermeir, S.; Vergauwe, N.; Verboven, P.; Nicolaï, B.; Lammertyn, J. Design and Optimization of a Double-Enzyme Glucose Assay in Microfluidic Lab-on-a-Chip. *Biomicrofluidics* **2009**, *3*, 044103.
9. Huh, D.; Bahng, J. H.; Ling, Y.; Wei, H.; Kripfgans, O. D.; Fowlkes, J. B.; Grotberg, J. B.; Takayama, S. Gravity-Driven Microfluidic Particle Sorting Device with Hydrodynamic Separation Amplification. *Anal. Chem.* **2007**, *79*, 1369–1376.
10. Ng, A. H. C.; Choi, K.; Luoma, R. P.; Robinson, J. M.; Wheeler, A. R. Digital Microfluidic Magnetic Separation for Particle-Based Immunoassays. *Anal. Chem.* **2012**, *84*, 8805–8812.
11. Destgeer, G.; Lee, K. H.; Jung, J. H.; Alazzam, A.; Sung, H. J. Continuous Separation of Particles in a PDMS Microfluidic Channel *via* Travelling Surface Acoustic Waves (TSAW). *Lab Chip* **2013**, *13*, 4210–4216.
12. Jellema, L. C.; Mey, T.; Koster, S.; Verpoorte, E. Charge-Based Particle Separation in Microfluidic Devices using Combined Hydrodynamic and Electrokinetic Effects. *Lab Chip* **2009**, *9*, 1914–1925.
13. Sugiyama, D.; Teshima, Y.; Yamanaka, K.; Briones-Nagata, M. P.; Maeki, M.; Yamashita, K.; Takahashi, M.; Miyazaki, M. Simple Density-Based Particle Separation in a Microfluidic Chip. *Anal. Methods* **2014**, *6*, 308–311.
14. Alrifaiy, A.; Lindahl, O. A.; Ramser, K. Polymer-Based Microfluidic Devices for Pharmacy, Biology and Tissue Engineering. *Polymers* **2012**, *4*, 1349–1398.
15. Lee, H. S.; Chu, W. K.; Zhang, K.; Huang, X. Microfluidic Devices with Permeable Polymer Barriers for Capture and Transport of Biomolecules and Cells. *Lab Chip* **2013**, *13*, 3389–3397.
16. Fu, J.; Mao, P.; Han, J. Artificial Molecular Sieves and Filters: A New Paradigm for Biomolecule Separation. *Trends Biotechnol.* **2008**, *26*, 311–320.

17. Masaeli, M.; Sollier, E.; Amini, H.; Mao, W.; Camacho, K.; Doshi, N.; Mitragotri, S.; Alexeev, A.; Di Carlo, D. Continuous Inertial Focusing and Separation of Particles by Shape. *Phys. Rev. X* **2012**, *2*, 031017.
18. Ito, Y.; Shinomiya, K. A New Continuous-Flow Cell Separation Method Based on Cell Density: Principle, Apparatus, and Preliminary Application to Separation of Human Buffy Coat. *J. Clin. Apheresis* **2001**, *16*, 186–191.
19. Kwon, K. W.; Choi, S. S.; Lee, S. H.; Kim, B.; Lee, S. N.; Park, M. C.; Kim, P.; Hwang, S. Y.; Suh, K. Y. Label-Free, Microfluidic Separation and Enrichment of Human Breast Cancer Cells by Adhesion Difference. *Lab Chip* **2007**, *7*, 1461–1468.
20. Cui, H.; Voldman, J.; He, X.; Lim, K. Separation of Particles by Pulsed Dielectrophoresis. *Lab Chip* **2009**, *9*, 2306–2312.
21. Gascoyne, P. R. C.; Vykoukal, J. Particle Separation by Dielectrophoresis. *Electrophoresis* **2002**, *23*, 1973–1983.
22. Weigl, B. H.; Yager, P. Microfluidic Diffusion-Based Separation and Detection. *Science* **1999**, *283*, 346–347.
23. Wang, W.; Duan, W.; Ahmed, S.; Mallouk, T. E.; Sen, A. Small Power: Autonomous Nano- and Micromotors Propelled by Self-Generated Gradients. *Nano Today* **2013**, *8*, 531–554.
24. Wang, J. *Nanomachines: Fundamentals and Applications*; Wiley-VCH: Weinheim, Germany, 2013.
25. Volpe, G.; Buttinoni, I.; Vogt, D.; Kümmerer, H.-J.; Bechinger, C. Microswimmers in Patterned Environments. *Soft Matter* **2011**, *7*, 8810–8815.
26. Zhao, G.; Pumera, M. Marangoni Self-Propelled Capsules in a Maze: Pollutants 'Sense and Act' in Complex Channel Environments. *Lab Chip* **2014**, *14*, 2818–2823.
27. Hong, Y.; Blackman, N. M. K.; Kopp, N. D.; Sen, A.; Velegol, D. Chemotaxis of Nonbiological Colloidal Rods. *Phys. Rev. Lett.* **2007**, *99*, 178103.
28. Baraban, L.; Harazim, S. M.; Sanchez, S.; Schmidt, O. G. Chemotactic Behavior of Catalytic Motors in Microfluidic Channels. *Angew. Chem., Int. Ed.* **2013**, *52*, 5552–5556.
29. Pumera, M. Nanomaterials Meet Microfluidics. *Chem. Commun.* **2011**, *47*, 5671–5680.
30. Xi, W.; Solovev, A. A.; Ananth, A. N.; Gracias, D. H.; Sanchez, S.; Schmidt, O. G. Rolled-up Magnetic Microdrillers: Towards Remotely Controlled Minimally Invasive Surgery. *Nanoscale* **2013**, *5*, 1294–1297.
31. Muddana, H. S.; Sengupta, S.; Mallouk, T. E.; Sen, A.; Butler, P. J. Substrate Catalysis Enhances Single-Enzyme Diffusion. *J. Am. Chem. Soc.* **2010**, *132*, 2110–2111.
32. Yu, H.; Jo, K.; Kounovsky, K. L.; de Pablo, J. J.; Schwartz, D. C. Molecular Propulsion: Chemical Sensing and Chemotaxis of DNA Driven by RNA Polymerase. *J. Am. Chem. Soc.* **2009**, *131*, 5722–5723.
33. Gáspár, S. Enzymatically Induced Motion at Nano- and Microscale. *Nanoscale* **2014**, *6*, 7757–7763.
34. Sakaue, T.; Kapral, R.; Mikhailov, A. S. Nanoscale Swimmers: Hydrodynamic Interactions and Propulsion of Molecular Machines. *Eur. Phys. J. B* **2010**, *75*, 381–387.
35. Cressman, A.; Togashi, Y.; Mikhailov, A. S.; Kapral, R. Mesoscale Modeling of Molecular Machines: Cyclic Dynamics and Hydrodynamical Fluctuations. *Phys. Rev. E: Stat., Nonlinear, Soft Matter Phys.* **2008**, *77*, 050901.
36. Golestanian, R. Synthetic Mechanochemical Molecular Swimmer. *Phys. Rev. Lett.* **2010**, *105*, 018103.
37. Colberg, P. H.; Kapral, R. Ångström-Scale Chemically Powered Motors. *Europhys. Lett.* **2014**, *106*, 30004.
38. Sengupta, S.; Dey, K. K.; Muddana, H. S.; Tabouillot, T.; Ibele, M. E.; Butler, P. J.; Sen, A. Enzyme Molecules as Nanomotors. *J. Am. Chem. Soc.* **2013**, *135*, 1406–1414.
39. Sengupta, S.; Spiering, M. M.; Dey, K. K.; Duan, W.; Patra, D.; Butler, P. J.; Astumian, R. D.; Benkovic, S. J.; Sen, A. DNA Polymerase as a Molecular Motor and Pump. *ACS Nano* **2014**, *8*, 2410–2418.
40. Switala, J.; Loewen, P. C. Diversity of Properties among Catalases. *Arch. Biochem. Biophys.* **2002**, *401*, 145–154.
41. Blakeley, R. L.; Webb, E. C.; Zerner, B. Jack Bean Urease (EC 3.5.1.5). A New Purification and Reliable Rate Assay. *Biochemistry* **1969**, *8*, 1984–1990.
42. Gossett, D. R.; Weaver, W. M.; Mach, A. J.; Hur, S. C.; Tse, H. T. K.; Lee, W.; Amini, H.; Di Carlo, D. Label-Free Cell Separation and Sorting in Microfluidic Systems. *Anal. Bioanal. Chem.* **2010**, *397*, 3249–3267.
43. Steinberg, G.; Schliwa, M. Characterization of the Biophysical and Motility Properties of Kinesin from the Fungus *Neurospora crassa*. *J. Biol. Chem.* **1996**, *271*, 7516–7521.
44. Jeon, N. L.; Dertinger, S. K. W.; Chiu, D. T.; Choi, I. S.; Stroock, A. D.; Whitesides, G. M. Generation of Solution and Surface Gradients using Microfluidic Systems. *Langmuir* **2000**, *16*, 8311–8316.
45. Xia, Y.; Whitesides, G. M. Soft Lithography. *Annu. Rev. Mater. Sci.* **1998**, *28*, 153–184.
46. Sia, S. K.; Whitesides, G. M. Microfluidic Devices Fabricated in Poly(Dimethylsiloxane) for Biological Studies. *Electrophoresis* **2003**, *24*, 3563–3576.